Role of Ag^+ in the Band Structures and Photocatalytic Properties of $AgMO_3$ (M: Ta and Nb) with the Perovskite Structure

Hideki Kato,[†] Hisayoshi Kobayashi,[‡] and Akihiko Kudo*[,†]

Department of Applied Chemistry, Faculty of Science, Science University of Tokyo, 1-3 Kagurazaka, Shinjuku-ku, Tokyo 162-8601, Japan, and Department of Chemistry and Bioscience, Faculty of Chemical Technology, Kurashiki University of Science and the Arts, 2640 Nishinoura, Tsurajima, Kurashiki 712-8505, Japan

Received: April 19, 2002; In Final Form: August 19, 2002

Photophysical and photocatalytic properties of perovskite-type materials $AgMO_3$ (M: Ta and Nb) consisting of Ag^+ and d^0 ions were investigated. The band gaps of $AgTaO_3$ and $AgNbO_3$ were 3.4 and 2.8 eV, respectively, being 0.6 eV smaller than the band gaps of $NaTaO_3$ (4.0 eV) and $NaNbO_3$, even if the crystal structures of $AgMO_3$ were similar to those of $NaMO_3$. It was found from the electronic band structure study, using the plane-wave-based density functional method, that a hybrid orbital of Ag 4d and O 2p formed a valence band at a more negative level than O 2p orbitals. $AgTaO_3$ showed photocatalytic activity for pure water splitting into H_2 and O_2 under UV-light irradiation. $AgNbO_3$ has arisen as a new visible-light-driven photocatalyst possessing the ability to evolve H_2 or O_2 from water in the presence of sacrificial reagents.

1. Introduction

The development of photocatalysts with visible-light response has been studied extensively from the viewpoint of the utilization of solar light energy. Doping of a foreign element into active photocatalysts with wide band gaps is the well-studied way to design the visible-light-driven photocatalyst. We have recently reported that $SrTiO_3$ and TiO_2 codoped with Cr^{3+} and Sb^{5+} showed photocatalytic activity for H_2 and O_2 evolution from aqueous solutions containing sacrificial reagents.[1] However, it may be considered that the doping of a foreign element is sometimes disadvantageous to designing visible-light-driven photocatalysts judging from the following reasons: (i) the dopant element works as an electron−hole recombination center, (ii) the mobility of electrons or holes in the dopant level is small because the dopant forms not a band but a discrete level, and (iii) the discrete dopant level hardly forms the active site for O_2 formation accompanied by four-electron oxidation.

WO_3 is a well-known visible-light-driven photocatalyst in which the valence band consists of O 2p orbitals for O_2 evolution from water containing sacrificial reagents.[2,3] WO_3 is not active for H_2 formation because of the low potential of the conduction band. Pt/CdS[3] and $BiVO_4$[4−6] have been reported to be visible-light-driven photocatalysts for H_2 and O_2 evolution from water containing sacrificial reagents. Their valence bands are formed by S 3p orbitals and the hybrid orbital of Bi 6s and O 2p, respectively. Although some sulfide photocatalysts have valence bands consisting of S 3p orbitals in a favorable position for O_2 formation, the holes photogenerated in the valence bands cause photocorrosion instead of the oxidation of water. In contrast, in the case of $BiVO_4$, the valence band consisting of the hybrid orbital of Bi 6s and O 2p is stable enough to oxidize water to form O_2. However, $BiVO_4$ cannot produce H_2 because of the low potential of the conduction band consisting of V 3d orbitals.[4,5] Therefore, making a stable valence band in a more negative position than O 2p orbitals and maintaining a conduction band level high enough to reduce water are indispensable to the development of visible-light-driven photocatalysts that possess the ability to form H_2 and O_2.

We have paid attention to Ag^+ as a candidate that forms a valence band. The standard redox potential of Ag^{2+}/Ag^+ is 1.98 V versus NHE. It indicates the possibility that Ag^+ in a crystal structure make a valence band at a more negative level than O 2p orbitals but at a more positive level than water oxidation to form O_2. Therefore, an investigation of the band structures of materials consisting of Ag^+ is worthwhile in order to develop new visible-light-driven photocatalysts for H_2 and O_2 evolution.

However, many of the active photocatalysts for water splitting such as $SrTiO_3$,[7] $K_2La_2Ti_3O_{10}$,[7] $KTaO_3$,[8,9] $NaTaO_3$,[10] $Sr_2M_2O_7$ (M: Ta and Nb),[9,11] and $RbNdTa_2O_7$[12] have perovskite-type structures that consist of corner-shared MO_6 octahedra. This suggests that compounds with perovskite structures are candidates for active photocatalyst materials. Silver tantalate $AgTaO_3$ has the same perovskite-type structure as $NaNbO_3$.[13] The Ta−O−Ta bond angle of the $AgTaO_3$ framework is 164°,[14] and it is close to that of $NaTaO_3$ (163°),[15] which is the most active photocatalyst among the tantalates. This interests us in the investigation into the band structure and the photocatalytic properties of $AgTaO_3$.

In the present study, the band structures and the photocatalytic properties of the perovskite-type materials ($AgMO_3$ (M: Ta and Nb)) consisting of Ag^+ were investigated, and the role of Ag^+ in the band structure was also discussed.

2. Experimental Section

$AgMO_3$ (M: Ta and Nb) powders were prepared by conventional solid-state reactions. Starting materials—Ag_2O (Kanto Chemical; 99.8%, 1−5 μm), Ta_2O_5 (Rare Metallic; 99.99%, 0.2−0.5 μm), and Nb_2O_5 (Kanto Chemical; 99.95%, 1−3 μm)—were mixed in a stoichiometric ratio or in the presence of excess amounts (2−5 mol %) of silver. The mixtures were calcined at

* To whom correspondence should be addressed. E-mail: a-kudo@rs.kagu.tus.ac.jp. Fax: +81-33235-2214.
[†] Science University of Tokyo.
[‡] Kurashiki University of Science and the Arts.

10.1021/jp025974n CCC: $22.00
Published on Web 11/12/2002

1350 K for 5 h for $AgTaO_3$ and at 1150 K for 5 h for $AgNbO_3$ in air using alumina crucibles (purity: 99.7%). In some cases, the obtained powders were treated with concentrated nitric acid to remove the excess silver. The obtained powders were confirmed by X-ray diffraction (Rigaku; RINT-1400). The commercial WO_3 powder (Nacali Tesque; 99.5%) was used to compare the photocatalytic activities. A NiO co-catalyst was loaded by an impregnation method from an aqueous solution of $Ni(NO_3)_2 \cdot 6H_2O$ (Wako Pure Chemical; 98.0%). The $AgTaO_3$ powder (0.5 g) and a small amount of water (ca. 1 mL) containing the appropriate amount of $Ni(NO_3)_2 \cdot 6H_2O$ were put into a porcelain crucible. Water was evaporated on a water bath. The suspension was stirred using a glass rod during the evaporation. The dried powder was calcined at 540 K for 1 h in air using a muffle furnace. A Pt co-catalyst was loaded by the photoreduction method. An aqueous solution containing an appropriate amount of $H_2PtCl_6 \cdot 6H_2O$ (Tanaka Kikinzoku; 37.55% as Pt) was added in 10 vol % methanol solution of the reactant solution. All of the $PtCl_6^{2-}$ in the reactant solution should be deposited on photocatalysts as metallic Pt islands by photoreduction under the band-gap irradiation.

Photocatalytic reactions were carried out in a suspended system and in the gas phase using a gas-closed circulation system. Photocatalytic H_2 evolution from the mixture of water (20 Torr) and methanol (70 Torr) vapor was also carried out in the gas phase. A top window cell made of Pyrex and a 300-W Xe lamp (ILC technology; CERMAX LX-300) were employed. In the case of the suspended system, the photocatalyst powder (0.15−0.3 g) was dispersed in a reactant solution (150 mL) by a magnetic stirrer in the cell. In the case of the gas−solid-phase reaction, the photocatalyst powder (1 g) was scattered on the bottom of the cell, and the gaseous mixture of water (20 Torr) and methanol (70 Torr) vapor was introduced into the system. The amounts of H_2 and O_2 that evolved were determined using gas chromatography (Shimadzu; GC-8A, MS-5A column, TCD, Ar carrier).

Diffuse reflection spectra were obtained using a UV−vis−NIR spectrometer (Jasco; UbestV-570) and were converted from reflection to absorbance by the Kubelka−Munk method. Photoluminescence was measured in vacuo using a spectrofluorometer (Spex; FluoroMax). Surface areas were determined by BET measurements (Coulter; SA3100). Photocatalyst powders were observed by a scanning electron microscope (Hitachi; S-5000). X-ray photoelectron spectra were measured using an X-ray photoelectron spectrometer (Shimadzu; ESCA-3200). Elemental analyses were carried out using an X-ray spectrofluorometer (JEOL; JSX-3200).

3. Calculation Method

The plane-wave-based density functional method calculation was carried out for $AgTaO_3$ and $NaTaO_3$ by employing the CASTEP program.[16] The core electrons were replaced with ultrasoft core potentials, and the valence electronic configurations for Ag, Ta, Na, and O atoms are $4d^{10}5s^1$, $6s^25d^3$, $2s^22p^6$-$3s^1$, and $2s^22p$,[4] respectively. The kinetic energy cutoffs were taken to be 260 and 280 eV for $AgTaO_3$ and $NaTaO_3$, respectively. The calculations were carried out using the conventional unit cells of $[AgTaO_3]_6$ and $[NaTaO_3]_4$, , which had 102 and 64 occupied orbitals, respectively. Table 1 shows the crystal parameters for both $[AgTaO_3]_6$ and $[NaTaO_3]_4$.

4. Results and Discussion

4.1. Photophysical Properties of $AgMO_3$ (M: Ta and Nb). Figure 1 shows X-ray diffraction patterns of $AgTaO_3$, $NaTaO_3$, and $KTaO_3$. All materials showed perovskite-type diffraction patterns though each material had a different peak position. The peaks of $KTaO_3$ were observed at the lowest angle. The peaks of $AgTaO_3$ were observed at a slightly lower angle than those of $NaTaO_3$. The differences in the peak position were due to the differences in the ionic radii of the cations ($K^+ \gg Ag^+ > Na^+$) occupying the A site of the perovskite structure. The bond angles (Ta−O−Ta) of the framework consisting of TaO_6 units in $AgTaO_3$, $NaTaO_3$, and $KTaO_3$ are 164,[14] 163,[15] and 180°,[17] respectively. Therefore, the structural properties of $AgTaO_3$ are between those of $NaTaO_3$ and $KTaO_3$ and rather close to those of $NaTaO_3$. It has been reported that the structure of $AgNbO_3$ is also similar to that of $NaNbO_3$.[13]

TABLE 1: Parameters of the Crystal Structures of $AgTaO_3$[14] and $NaTaO_3$[15]

$AgTaO_3$			
system: trigonal	a: 5.528		α: 90.0
space group: R-3c	b: 5.528		β: 90.0
	c: 13.716		γ: 120.0
atom positions	x	y	z
Ag	0	0	0.25
Ta	0	0	0
O	0.5546	0	0.25

$NaTaO_3$			
system: orthorhombic	a: 5.513		α: 90.0
space group: Pcmn	b: 7.751		β: 90.0
	c: 5.494		γ: 90.0
atom positions	x	y	z
Na	0	0.25	−0.02
Ta	0	0	0.5
O	0.054	0.25	0.5
O	0.275	−0.027	0.275

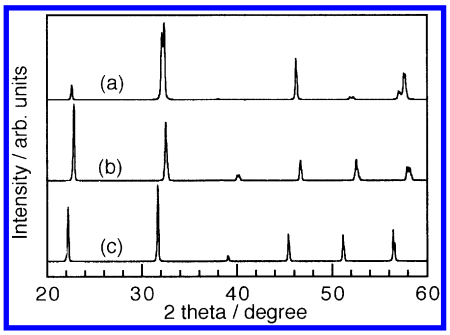

Figure 1. X-ray diffraction patterns of perovskite-type tantalates (a) $AgTaO_3$, (b) $NaTaO_3$, and (c) $KTaO_3$.

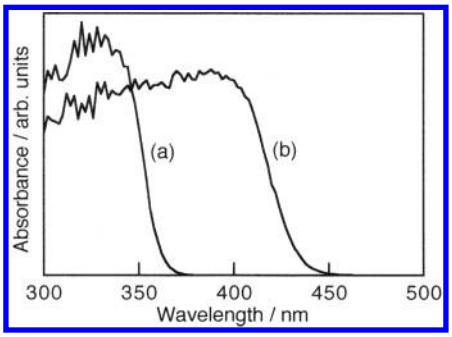

Figure 2. Diffuse reflection spectra of (a) $AgTaO_3$ and (b) $AgNbO_3$.

Figure 2 shows diffuse reflection spectra of $AgTaO_3$ and $AgNbO_3$. The band gaps of $AgTaO_3$ and $AgNbO_3$ were estimated to be 3.4 and 2.8 eV, respectively, from the onsets of

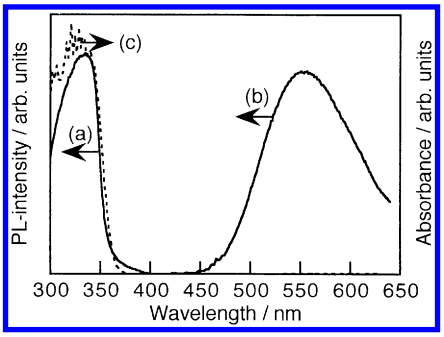

Figure 3. Photoluminescence spectra of $AgTaO_3$ at 77 K; (a) an excitation spectrum monitored at 550 nm, (b) an emission spectrum excited at 340 nm, and (c) a diffuse reflection spectrum at 300 K.

TABLE 2: Photophysical Properties of $AgTaO_3$ and Alkali Tantalates

catalyst	Ta−O−Ta bond angle/ (deg)	band gap[a]/ eV	emission max.[b]/ nm	stokes shift/ 10^3 cm^{-1}
$AgTaO_3$	164	3.4	550	11.2
$LiTaO_3$	143	4.7	360	13.6
$NaTaO_3$	163	4.0	463	12.7
$KTaO_3$	180	3.6	510	10.3

[a] Estimated from the onset of absorption. [b] Observed at 77 K.

absorption. The $AgTaO_3$ powder was white whereas the $AgNbO_3$ powder was pale yellow.

$AgTaO_3$ showed photoluminescence at 77 K, as shown in Figure 3. The excitation spectrum agreed well with the diffuse reflection spectrum. The photophysical properties of $AgTaO_3$ and the alkali tantalates are summarized in Table 2. The Stokes shift of $AgTaO_3$ was 11.2×10^3 cm^{-1}. However, no photoluminescence was observed for $AgNbO_3$. It has been reported by Wiegel et al. that in alkali tantalates, as the Ta−O−Ta bond angle in a perovskite framework gets close to 180°, the band gap becomes smaller, and the delocalization of the excited energy is larger.[18] The band gap of $AgTaO_3$ was 0.6 eV smaller than that of $NaTaO_3$, even if the bond angle of $AgTaO_3$ was close to that of $NaTaO_3$.[14,15] The result did not abide by the relationship between the TaO_6 framework and the band gap. Similarly, the band gap of $AgNbO_3$ was 0.6 eV smaller than that of $NaNbO_3$. However, the Stokes shift of $AgTaO_3$ was between that of $KTaO_3$ and $NaTaO_3$, which indicated that the relationship between the TaO_6 framework and the energy delocalization was also adopted for $AgTaO_3$. Thus, it was found that Ag^+ in $AgTaO_3$ and $AgNbO_3$ made the band gaps decrease but did not affect the delocalization of the excited energy.

4.2. Band Structure of the $AgTaO_3$ Photocatalyst. The electronic structure of $AgTaO_3$ was studied by the plane-wave-based density functional method in order to clarify which Ag^+ contributed to valence- or conduction-band formation in the decrease of the band gap. Figure 4 shows the band structure and the density of states (DOS) of $AgTaO_3$ and $NaTaO_3$. Figure 5 shows the density contour maps for the LUMO and HOMO of $AgTaO_3$. Three occupied bands and two unoccupied bands are shown in the DOS diagram in Figure 4. An occupied band on the low-energy side consists of O 2s orbitals. The occupied band in the middle consists of only O 2p orbitals. The occupied band on the high-energy side (i.e., a valence band) consists of the hybrid orbital of Ag 4d and O 2p. The top of the valence band (HOMO) is shown in Figure 5b. In contrast, the contribution of Ag^+ was not observed for the bottom of the conduction band including the LUMO, and it consisted of only Ta 5d orbitals, as shown in Figure 5a. In particular, the t_{2g} orbitals seemed to form mainly on the bottom of the conduction band. Above the Ta 5d band, the Ag 5s and Ag 5p orbitals appeared in the unoccupied bands. In general, the valence bands of oxides with d^0 and d^{10} metal cations such as $NaTaO_3$ and $NaNbO_3$

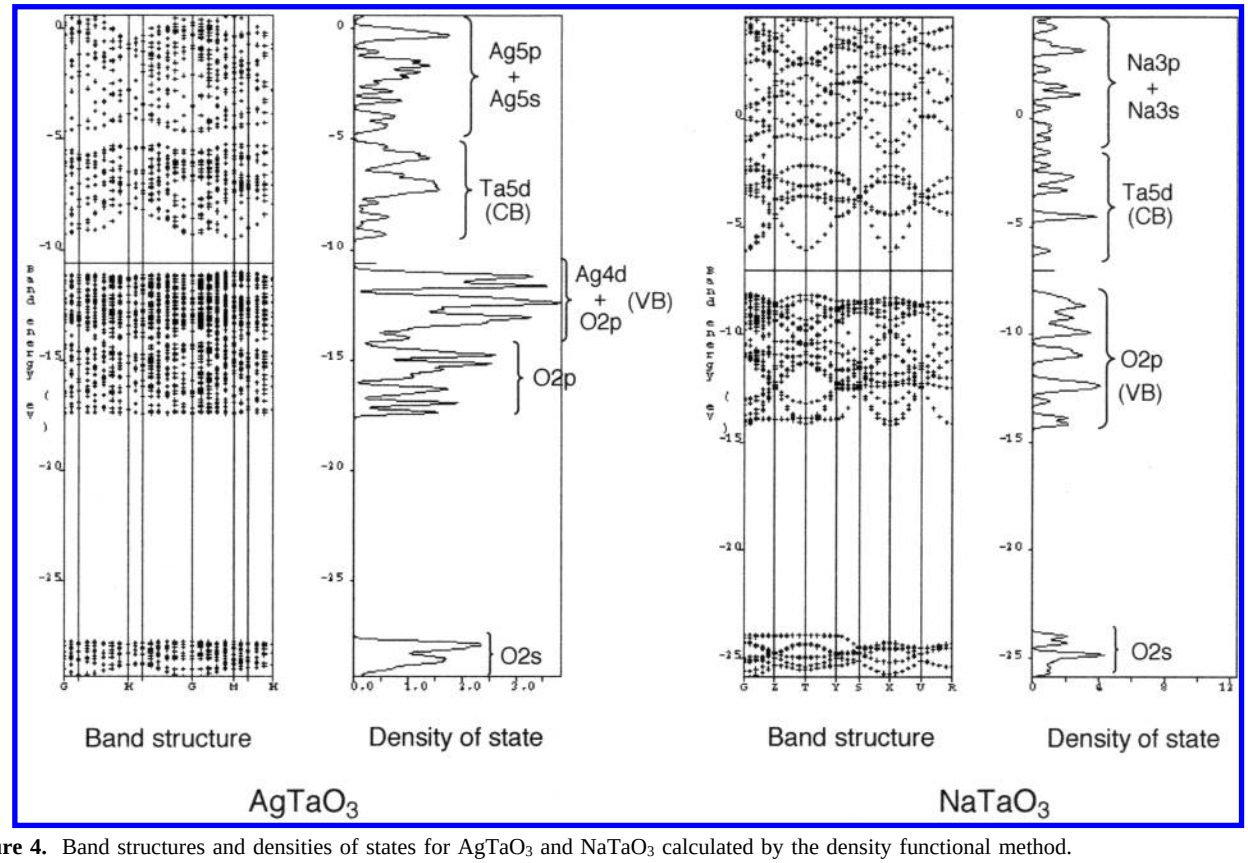

Figure 4. Band structures and densities of states for $AgTaO_3$ and $NaTaO_3$ calculated by the density functional method.

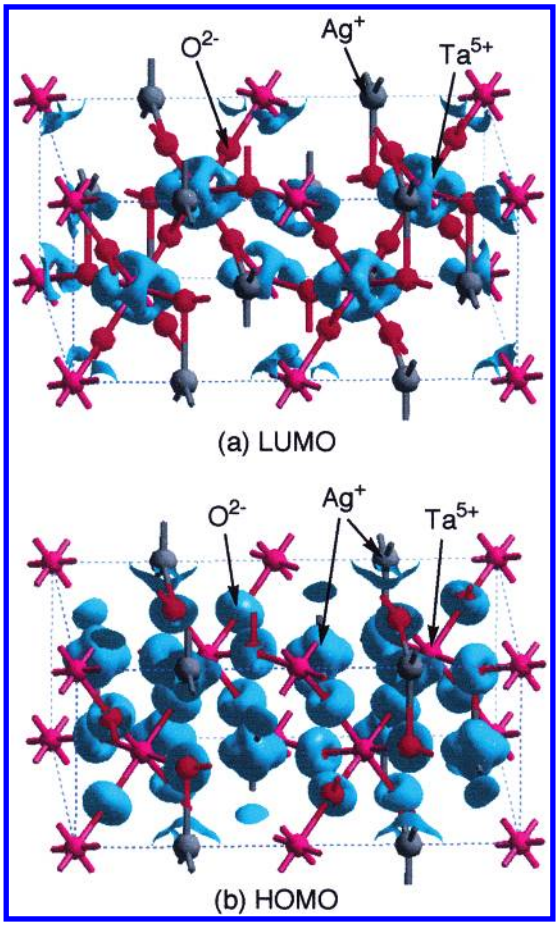

Figure 5. Density contour maps for the LUMO and HOMO of $AgTaO_3$.

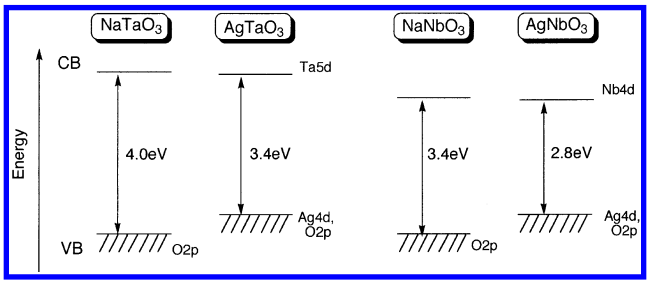

Figure 6. Band structures of $NaTaO_3$, $AgTaO_3$, $NaNbO_3$, and $AgNbO_3$.

consist of O 2p orbitals, and the potential is usually ca. 3 eV.[19] In contrast to them, it was revealed that the band gaps of $AgTaO_3$ and $AgNbO_3$ were 0.6 eV smaller than those of $NaTaO_3$ and $NaNbO_3$, respectively, because the Ag 4d orbitals made the valence bands at more negative levels than the O 2p orbitals. The crystal structures of $AgTaO_3$ and $AgNbO_3$ were similar to those of $NaTaO_3$ and $NaNbO_3$, respectively, as mentioned above. The conduction-band levels of $AgTaO_3$ and $AgNbO_3$ were estimated to be slightly lower than those of $NaTaO_3$ (−1.06 eV) and $NaNbO_3$ (−0.4 eV), judging from the bond angles of the TaO_6 framework. Therefore, the band structures of $AgTaO_3$ and $AgNbO_3$ could be illustrated as shown in Figure 6. Thus, it has been found that silver is one of the elements that is able to make a valence-band position higher than O 2p orbitals. This is noteworthy information needed in order to design new visible-light-driven photocatalysts.

4.3. Photocatalytic Activities of $AgTaO_3$ and $AgNbO_3$. The photocatalytic activity of $AgTaO_3$ is summarized in Table 3. $AgTaO_3$ showed activity for H_2 and O_2 evolution from aqueous solutions of methanol and silver nitrate under UV-light irradiation, respectively. Moreover, $AgTaO_3$ showed activity for water splitting into H_2 and O_2. The activity of $AgTaO_3$, prepared in the presence of an excess amount of silver, was higher than that of $AgTaO_3$, prepared in a stoichiometric ratio. Figure 7 shows scanning electron microscope images of $AgTaO_3$ prepared with and without an excess amount of silver. The particle size and surface area of $AgTaO_3$ powder were 0.5−1 μm and 1 m^2 g^{-1}, respectively. It seemed that the excess amount of silver did not affect the crystal shape and sizes. The volatilization of silver would occur during high-temperature calcination. There-

TABLE 3: Photocatalytic Activity of $AgTaO_3$

catalyst	ratio of Ag to Ta[a]	reaction solution	activity/ μmol h^{-1} H_2	O_2
$AgTaO_3$	1.00	0.05 M $AgNO_3$(aq)		22.2
Pt(0.5wt %)/$AgTaO_3$	1.00	10 vol % CH_3OH(aq)	13.1	
$AgTaO_3$	1.00	pure water	0.11	0.04
NiO(0.1wt %)/$AgTaO_3$	1.00	pure water	13	1.0
$AgTaO_3$	1.05	0.05 M $AgNO_3$(aq)		53.2
$AgTaO_3$	1.05	10 vol % CH_3OH(aq)	29.5	
NiO(0.3wt %)/$AgTaO_3$	1.05	10 vol % CH_3OH (aq)	96.5	
Pt(0.1wt %)/$AgTaO_3$	1.05	10 vol % CH_3OH(aq)	506	
$AgTaO_3$	1.05	pure water	1.4	0.3
NiO(0.3wt %)/$AgTaO_3$	1.05	pure water	16.1	5.6

[a] In the starting materials. Catalyst: 0.15−0.3 g; reactant solution: 150 mL, 300-W Xe lamp (λ > 300 nm), top window cell made of Pyrex.

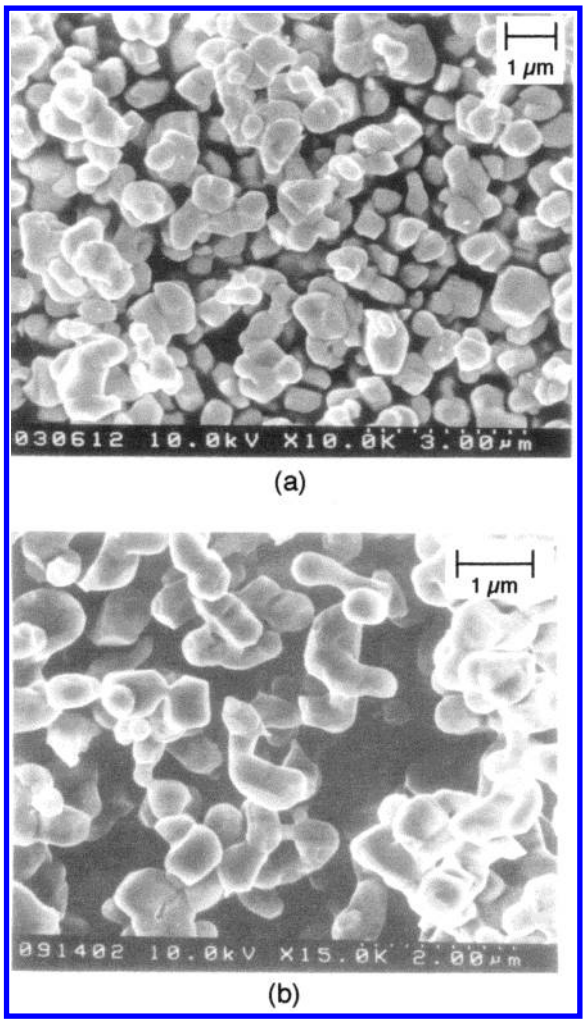

Figure 7. Scanning electron microscope images of $AgTaO_3$ prepared (a) without an excess amount of silver and (b) in the presence of 2 mol % of an excess amount of silver.

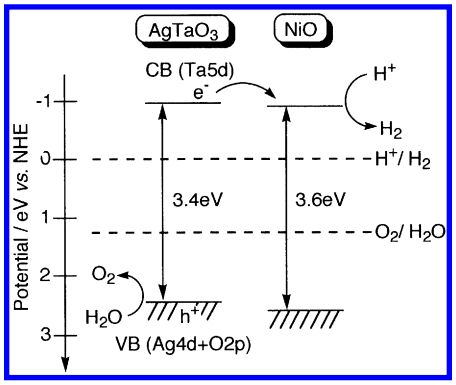

Figure 8. Scheme of photocatalytic water splitting on the $NiO/AgTaO_3$ photocatalyst.

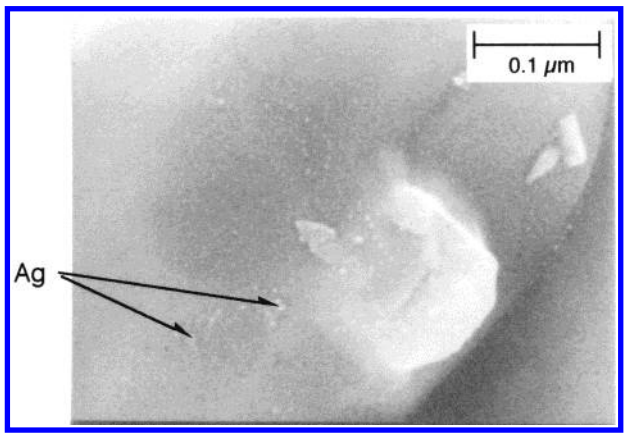

Figure 9. Scanning electron microscope image of metallic silver particles on $AgTaO_3$ prepared in the presence of 2 mol % of an excess amount of silver.

fore, silver defects would be formed in $AgTaO_3$ prepared in a stoichiometric ratio, resulting in low activity due to the increase in recombination between photogenerated electrons and holes as well as in the case of alkali tantalates.[10] Therefore, the enhancement of activity by the addition of an excess amount of silver might be due to the suppression of the formation of silver ion defects.

$AgTaO_3$ showed activity for H_2 formation even without any co-catalysts such as Pt. The activity increased 17 times when a Pt co-catalyst was loaded. However, the activities for H_2 formation and water splitting of NiO-loaded $AgTaO_3$ were 3 times and 10 times higher, respectively, than those of native $AgTaO_3$, even without pretreatment. The results indicated that the electrons photogenerated in the conduction band of $AgTaO_3$ were able to transfer to the conduction band of NiO because the conduction-band level of $AgTaO_3$ was estimated to be higher than that of NiO (−0.96 eV)[20] as well as that of $NaTaO_3$, as shown in Figure 8. It is noteworthy that water splitting into H_2 and O_2 proceeded over the photocatalyst with the valence band consisting of orbitals other than O 2p orbitals.

A large number of metallic silver particles were observed on the surface of $AgTaO_3$ prepared in the presence of an excess amount of silver, as shown in Figure 9. The existence of metallic silver was also detected by XRD measurements. The electron migration to the metallic silver particles might decrease the photocatalytic activity. Therefore, the effect of treatment with concentrated nitric acid (to remove the metallic silver particles on the surface) upon the photocatalytic activity of $NiO/AgTaO_3$ was investigated (Table 4). All $NiO/AgTaO_3$ catalysts treated with acid showed higher activities than nontreated $NiO/AgTaO_3$ catalysts. $NiO/AgTaO_3$ treated with acid for 1 min after the loading of NiO showed the highest activity among all of the catalysts. The relative intensity of Ag3d/Ta4d in XPS for 1-min-treated $NiO/AgTaO_3$ was smaller than that of nontreated $NiO/AgTaO_3$, which indicates that the excess silver was removed even by short-time treatment with acid. As the acid-treatment time increased, the activity decreased, and the ratio of evolved H_2 to O_2 deviated from the stoichiometry. No difference was observed in the relative intensities of Ag3d/Ta4d in XPS between $NiO/AgTaO_3$ photocatalysts treated with acid for 1 min and 10 min. The O_2 formation sites (surface Ag^+) of $NiO/AgTaO_3$ might collapse during the long period of acid treatment, resulting in a deviation from the stoichiometry. The amounts of NiO loaded were also decreased by the acid treatment, but the loss was comparatively small. However, although the activities of $NiO/AgTaO_3$ treated with acid before the loading of NiO were also higher than those of nontreated $NiO/AgTaO_3$, the ratio of H_2/O_2 deviated from the stoichiometry more than that of $NiO/AgTaO_3$ treated with acid after the loading of NiO. In the acid treatment process, part of the surface silver ions were also eluted by the ion exchange with protons. In the case of acid treatment before the loading of NiO, dehydration would occur for $AgTaO_3$ with the partly protonated surface during the high-temperature calcination in the process of loading NiO. This dehydration causes the surface structure of $AgTaO_3$ to collapse. The NiO co-catalyst should work as an active site for H_2 evolution whereas the surface of $AgTaO_3$ would be for O_2 formation sites. Therefore, the destruction of the surface structure of acid-treated $AgTaO_3$ by heat treatment would cause the further destruction of the O_2 formation sites. The photocatalytic water splitting over $NiO/AgTaO_3$ treated with acid for 1 min after the loading of NiO is shown in Figure 10. Although the activity gradually decreased with irradiation time, it was recovered by the evacuation of the gas-phase products. Such deactivation and recovery of the activity were observed in all cases for water splitting using $AgTaO_3$ photocatalysts. Therefore, although the ratio of H_2/O_2 deviated from the stoichiometry, the reactions proceeded photocatalytically. The deviation of the ratio of H_2/O_2 from the stoichiometry seemed to be due to the adsorption of formed O_2 on the $AgTaO_3$ surface owing to a strong affinity between $AgTaO_3$ and O_2. The recovery of activity after the evacuation of gas-phase products would be due to the desorption of adsorbed O_2 from the $AgTaO_3$ surface. In the case of the most active photocatalyst, which was treated with acid for a short period of time(1 min) after the loading of NiO, although H_2 and O_2 finally evolved with a stoichiometry within the experimental error (Table 4 and Figure 10), the amount of evolved O_2 was also small in the initial stage. This result also supported the adsorption of formed O_2. The amounts of H_2 and

TABLE 4: Effect of Acid Treatment for NiO(0.30 wt %)/ $AgTaO_3$ on Photocatalytic Activity for Water Splitting

treatment with concentrated HNO_3	treatment time/min	amount of NiO[a]/wt %	relative peak intensity in XPS Ag3d/Ta4d	activity/ μmol h^{-1}	
				H_2	O_2
after the loading of NiO	0	0.30	2.7	8.5	3.7
	1	0.24	1.7	20.7	9.5
	3	0.21		14.4	5.9
	10	0.19	1.7	14.1	5.5
before the loading of NiO	1	0.30		18.2	5.2
	30	0.30		16.1	5.6

[a] Determined by XRF. Catalyst: 0.15 g; pure water: 150 mL; 300-W Xe lamp (λ > 300 nm), top window cell made of Pyrex.

TABLE 5: Photocatalytic Activity of $AgNbO_3$

catalyst	ratio of Ag to Nb[a]	incident light/nm	reaction condition	activity/μmol h^{-1} H_2	activity/μmol h^{-1} O_2
$AgNbO_3$	1.00	>420	0.05 M $AgNO_3$(aq)		14
$AgNbO_3$	1.00	>300	0.05 M $AgNO_3$(aq)		119
Pt(0.05wt %)/$AgNbO_3$	1.00	>420	10 vol % CH_3OH(aq)	0.5	
Pt(0.05wt %)/$AgNbO_3$	1.00	>300	10 vol % CH_3OH(aq)	3.1	
$AgNbO_3$	1.05	>420	0.05 M $AgNO_3$(aq)		37.0
$AgNbO_3$	1.05	>300	0.05 M $AgNO_3$(aq)		240
Pt(0.1wt %)/$AgNbO_3$	1.05	>420	10 vol % CH_3OH(aq)	0.4	
Pt(0.1wt %)/$AgNbO_3$	1.05	>300	10 vol % CH_3OH(aq)	6.1	
$AgNbO_3$	1.05	>420	H_2O, CH_3OH vapor[b]	1.7	
Pt(0.1wt %)/$AgNbO_3$	1.05	>420	H_2O, CH_3OH vapor[b]	8.2	
Pt(0.1wt %)/$AgNbO_3$	1.05	>300	H_2O, CH_3OH vapor[b]	38.0	
WO_3		>420	0.05 M $AgNO_3$(aq)		47.6
WO_3		>300	0.05 M $AgNO_3$(aq)		269
Pt(0.1wt %)/WO_3		>420	H_2O, CH_3OH vapor[b]	0	
Pt(0.1wt %)/WO_3		>300	H_2O, CH_3OH vapor[b]	0.04	

[a] In the starting materials. [b] Pressure of H_2O and CH_3OH was 20 and 70 Torr, respectively. Catalyst: 0.3 g for liquid-phase reactions and 1.0 g for gas-phase reactions; reactant solution: 150 mL, 300-W Xe lamp, top window cell made of Pyrex.

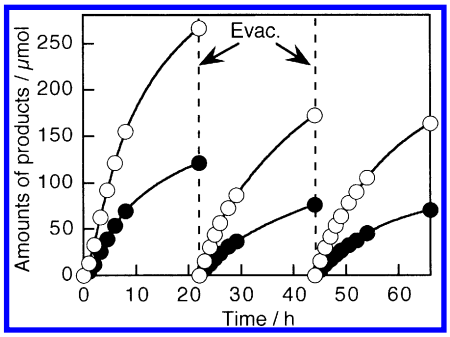

Figure 10. Photocatalytic water splitting into H_2 and O_2 over NiO-(0.3 wt %)/$AgTaO_3$ treated with concentrated HNO_3 for 1 min. Catalyst: 0.15 g; pure water: 150 mL; 300-W Xe lamp (λ > 300 nm), cell with a top window made of Pyrex.

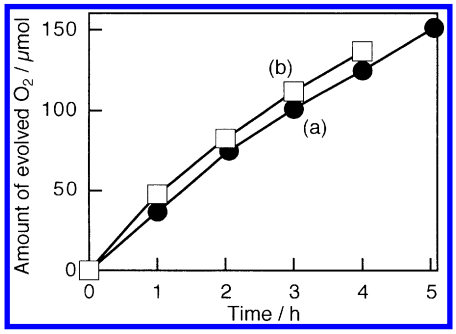

Figure 11. Photocatalytic O_2 evolution from an aqueous $AgNO_3$ solution over (a) $AgNbO_3$ and (b) WO_3 under visible-light irradiation. Catalyst: 0.3 g; an aqueous $AgNO_3$ solution: 0.05 mol L^{-1}, 150 mL; 300-W Xe lamp (λ > 420 nm), cell with a top window made of Pyrex.

O_2 evolved for 66 h of irradiation were 600 and 268 μmol, respectively. The turnover number of reacted electrons to the total amount of Ta in the catalyst used was 3. This indicates that the reaction proceeded photocatalytically on NiO/$AgTaO_3$.

Table 5 shows the photocatalytic activity of $AgNbO_3$. The particle size and surface area of $AgNbO_3$ powder were 2−4 μm and 0.5 m^2 g^{-1}, respectively. $AgNbO_3$ was hardly active for H_2 evolution from an aqueous methanol solution whereas it showed a high activity for O_2 evolution from an aqueous silver nitrate solution, even under visible-light irradiation. The photocatalytic activity of $AgNbO_3$ was also increased by the addition of an excess amount of silver in the preparation as well as for the case of $AgTaO_3$. Figure 11 shows photocatalytic O_2 evolution from an aqueous silver nitrate solution over

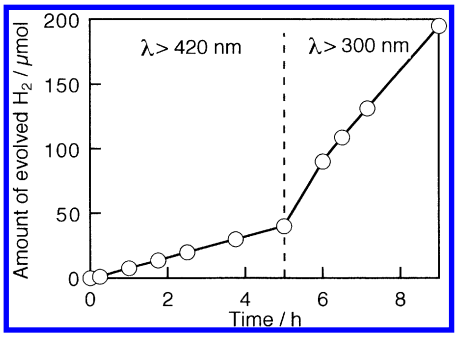

Figure 12. Photocatalytic H_2 evolution from a gaseous mixture of H_2O (20 Torr) and CH_3OH (70 Torr) over Pt(0.1 wt %)/$AgNbO_3$. Catalyst: 1.0 g; 300-W Xe lamp, cell with a top window made of Pyrex.

$AgNbO_3$ under visible-light irradiation (λ > 420 nm). The activity of $AgNbO_3$ was similar to that of WO_3, of which the band gap was the same as that for $AgNbO_3$. Although the activity of $AgNbO_3$ for H_2 evolution from an aqueous methanol solution was very low, $AgNbO_3$ showed a high activity for H_2 formation from the mixture of water and methanol vapor, as shown in Figure 12. The activity of the H_2 evolution of Pt/$AgNbO_3$ was gradually decreased. A long experiment was carried out to check the stability of the photocatalyst. Although the activity gradually decreased, the reaction became steady after 10 h of irradiation. Moreover, no difference before and after the photocatalytic H_2 evolution was observed in XRD patterns. Therefore, it was considered that the initial deactivation of the Pt/$AgNbO_3$ photocatalyst was not due to the reduction of Ag^+ in the catalyst. In contrast, WO_3, of which the conduction-band level is lower than the redox potential of H^+/H_2, showed no activity for H_2 evolution even in the gas−solid system. The band structure of $AgNbO_3$ can be drawn as Figure 13 in consideration of the results. The conduction-band level of $AgNbO_3$ was higher than that of WO_3 with the same band gap as $AgNbO_3$ and also higher than the redox potential of H^+/H_2. Thus, $AgNbO_3$ has been developed as a new visible-light-driven photocatalyst with the ability to form H_2 or O_2. The reason that the activity for H_2 evolution in the suspension system was low has not been clarified at the present stage.

5. Conclusions

The structural properties of $AgTaO_3$ are between those of $NaTaO_3$ and $KTaO_3$ and are close to those of $NaTaO_3$. In the

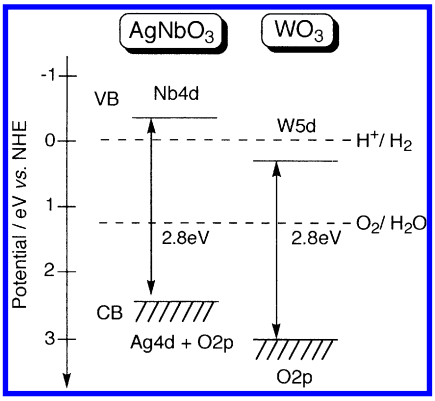

Figure 13. Energy diagrams of $AgNbO_3$ and WO_3 photocatalysts.

case of alkali tantalates, as the Ta−O−Ta bond angle gets close to 180°, the band gap becomes smaller. However, the band gap of $AgTaO_3$ was 3.4 eV, which was 0.6 eV smaller than that of $NaTaO_3$, even if the Ta−O−Ta bond angle of $AgTaO_3$ was close to that of $NaTaO_3$. In contrast, the value of the Stokes shift of $AgTaO_3$ was between that of $KTaO_3$ and $NaTaO_3$. The band gap of $AgNbO_3$ was also 0.6 eV smaller than that of $NaNbO_3$. It was indicated from the electronic structure study of $AgTaO_3$ by the density functional method that the hybrid of Ag 4d and O 2p orbitals formed the valence band at a more negative level than the O 2p orbitals, resulting in a decrease in the band gap.

$AgTaO_3$ showed photocatalytic activity for H_2 and O_2 evolution from water containing sacrificial reagents under UV irradiation. Moreover, $AgTaO_3$ showed activity for water splitting into H_2 and O_2. The activity increased by 1 order of magnitude when a NiO co-catalyst was loaded. However, $AgNbO_3$ showed photocatalytic activity for O_2 evolution from an aqueous silver nitrate solution and H_2 formation from a mixture of water and methanol vapor under visible-light irradiation. Thus, $AgNbO_3$ was developed to be a new visible-light-driven photocatalyst with the ability to form H_2 or O_2.

Acknowledgment. We thank Professor K. Domen (Chemical Resources Laboratory, Tokyo Institute of Technology) for XPS measurements. This work was supported by Core Research for Evolutional Science and Technology (CREST) and the Tokyo Ohka Foundation for the Promotion of Science and Technology. H.K. has been awarded a research fellowship by the Japan Society for the Promotion of Science for Young Scientists.

References and Notes

(1) Kato, H.; Kudo, A. *J. Phys. Chem. B* **2002**, *106*, 5029.

(2) Darwent, J. R.; Mills, A. *J. Chem. Soc., Faraday. Trans. 2* **1982**, *78*, 359.

(3) Sakata, T. Heterogeneous Photocatalysis at Liquid−Solid Interfaces. In *Photocatalysis*; Serpone, N., Pelizzetti, E., Eds.; Wiley: New York, 1989; Chapter 10, pp 311−338.

(4) Kudo, A.; Ueda, K.; Kato, H.; Mikami, I. *Catal. Lett.* **1998**, *53*, 229.

(5) Kudo, A.; Omori, K.; Kato, H. *J. Am. Chem. Soc.* **1999**, *121*, 11459.

(6) Tokunaga, S.; Kato, H.; Kudo, A. *Chem. Mater.* **2001**, *13*, 4624.

(7) Domen, K.; Kondo, J. N.; Hara, M.; Takata, T. *Bull. Chem. Soc. Jpn.* **2000**, *73*, 1307, and references therein.

(8) Ishihara, T.; Nishiguchi, H.; Fukamachi, K.; Takita, Y. *J. Phys. Chem. B* **1999**, *103*, 1.

(9) Kudo, A. *J. Ceram. Soc. Jpn.* **2001**, *109*, S81, and references therein.

(10) Kato, H.; Kudo, A. *J. Phys. Chem. B* **2001**, *105*, 4285.

(11) Hwang, D. W.; Kim, H. G.; Kim, J.; Cha, K. Y.; Kim, Y. G.; Lee, J. S. *J. Catal.* **2000**, *193*, 40.

(12) Machida, M.; Yabunaka, J.; Kijima, T. *Chem. Mater.* **2000**, *12*, 812.

(13) Francombe, M. H.; Lewis, B. *Acta Crystallogr.* **1958**, *11*, 175.

(14) Wolcyrz, M.; Lukaszewski, M. *Z. Kristallogr.* **1986**, *177*, 53.

(15) Ahtee, M.; Unonius, L. *Acta Crystallogr., Sect. A* **1977**, *33*, 150.

(16) Payne, M. C.; Teter, M. P.; Allan, D. C.; Arias, T. A.; Joannopoulos, J. D. *Rev. Mod. Phys.* **1992**, *64*, 1045.

(17) Zhurova, E. A.; Zavodnik, V. E.; Trirel'son, V. G. *Kristallografiya* **1995**, *40*, 816.

(18) Wiegel, M.; Emond, M. H. J.; Stobbe, E. R.; Blasse, G. *J. Phys. Chem. Solids* **1994**, *55*, 773.

(19) Scaife, D. E. *Sol. Energy* **1980**, *25*, 41.

(20) Dare-Edwards, M. P.; Goodenough, J. B.; Hamnett, A.; Nicholson, N. D. *J. Chem. Soc., Faraday Trans. 2* **1981**, *77*, 643.